Collective radial breathing modes in homogeneous nanotube bundles

Charlotte Berrezueta-Palacios [a,*], Dekel Nakar [b], Anna Wroblewska [c], Oisín Garrity [a], Han Li [d,e], Nitzan Shadmi [b], Benjamin S. Flavel [d], Ernesto Joselevich [b], Stephanie Reich [a,*], Georgy Gordeev [a,f,*]

[a] Department of Physics, Freie Universität Berlin, Berlin 14195, Germany
[b] Department of Molecular Chemistry and Materials Science, Weizmann Institute of Science, Rehovot 7610001, Israel
[c] Faculty of Physics, Warsaw University of Technology, Koszykowa 75, 00-662, Warsaw, Poland
[d] Institute of Nanotechnology, Karlsruhe Institute of Technology, Kaiserstraße 12, 76131 Karlsruhe, Germany
[e] Department of Mechanical and Materials Engineering, University of Turku, Vesilinnantie 5, 20500 Turku, Finland
[f] Department of Physics and Materials Science, University of Luxembourg, L-4422 Belvaux, Luxembourg

Keywords:
Collective vibrational modes
Carbon nanotube bundles
Radial breathing modes
Nanotube bundles
Nanotube films
Phononic crystals

A B S T R A C T

We present a Raman study of the collective vibrations arising from the homogeneous bundling of single-walled carbon nanotubes and analyze the dependence of their vibrational coupling on the tube diameter using two systems, single-walled carbon nanotube coils and a monochiral carbon nanotube film. We report on two breathing-like modes for quasi-infinite bundles, compared to the single radial breathing mode characteristic for isolated tubes. The exciton-phonon coupling in these modes is probed with resonant Raman spectroscopy, revealing the same resonance energy for both breathing-like peaks. Our experimental findings align well with previously reported theoretical studies, demonstrating a $1/d$ scaling for all modes, as well as confirming the relative shift of the modes dependent on intertube interaction. These vibrations provide insight into the role of intertube lattice dynamics in two-dimensional THz-range phononic crystals.

1. Introduction

The vibrational properties of solids regulate their mechanical properties, excited state relaxation, thermal and electrical conductivity. To tailor these properties, the concept of phononic crystal has been proposed [1,2]. In a phononic crystal, building blocks with different elastic moduli are periodically arranged [3] and their collective behavior may realize exotic vibrational states, including phononic band gaps [4–7] and topological wave propagation [5,8–11]. One of the strategies suggested to create phononic crystals is to arrange one-dimensional cylinders into a superlattice, producing an additional two-dimensional reciprocal lattice in the directions perpendicular to the axis of the cylinders [3,12]. Up to now, this approach has been limited to acoustic modes with eigenfrequencies measured in the kHz range. To reach the desirable THz regime with this concept, the unit size should be decreased and the elastic constants increased [13]. This can be achieved with single-walled carbon nanotubes (SWCNTs), tubular monolayers of sp^2 carbon with diameters down to 0.5 nm [14] and radial elastic moduli up to 57 GPa [15].

SWCNTs form wall-to-wall aggregates naturally and arrange into supercrystals with a (close-pack) hexagonal symmetry, where their breathing vibrational modes are modulated by the van der Waals potential between the tube walls. The properties of such carbon nanotube (CNT) crystals depend on their packing density and chiral purity. Homogeneous bundles consisting of only one type of CNT with the same electronic structure promote electron mobility and enhance the long-distance coherence in intertube interaction, leading to perfect crystalline behavior. Previous studies observed a decrease in the band gap for semiconducting nanotubes [16,17] and the formation of intertube excitons [18,19]. For such artificial crystals, novel vibrational effects were predicted such as soliton waves [20] and new vibrational modes that are absent in individual tubes [21,22]. Despite these theoretical proposals, none of the additional vibrations have been observed experimentally so far.

Here, we present a Raman study of the collective vibrational modes in hexagonally-packed CNTs in the form of homogeneous coils and films. Their vibrational properties are compared to the modes of individual tubes. The homogeneous bundling yields additional Raman-active modes in the low-frequency region (below 500 cm^{-1}). We report on two modes (RBM_{B1}) and (RBM_{B2}) for quasi-infinite bundles, compared to the single radial breathing mode (RBM) characteristic of

* Corresponding authors.
E-mail addresses: charlotte.berrezueta@fu-berlin.de (C. Berrezueta-Palacios), reich@physik.fu-berlin.de (S. Reich), georgy.gordeev@uni.lu (G. Gordeev).

isolated tubes. Resonant Raman spectroscopy confirms that both modes originate from the same nanotube chirality. Our experimental data on three CNT bundles, each consisting of a different tube diameter, confirm the theoretical predictions of lattice dynamics for infinite nanotube bundles with identical chiralities, as well as the diameter dependence of the vibrational coupling. These results reveal the role of intertube lattice dynamics in carbon nanotube bundles due to the emergence of collective vibrations.

2. Experimental details

We adopt two approaches for the creation of homogeneous ensembles of nanotubes: (a) the self-winding of a single-walled carbon nanotube into a coil during its growth [17,23] and (b) a film of pre-sorted and enriched monochiral CNT solution through vacuum filtration [24]. Both approaches yield highly pure material, which provides a suitable platform for studying collective vibrations in homogeneous CNT bundles. The particular strength of the coiled tubes lies not only in their singular chirality but also in their single-handedness composition. In contrast, the (6,5) film contains both left and right-handed chiralities. However, we do not expect this to have a major effect on the low-frequency vibrations of the RBM, which mainly probe the mechanical response of the tube.

Coil samples were obtained by chemical vapor deposition (CVD) synthesis of carbon nanotubes on a Si/SiO_2 substrate using a catalyst of ferric chloride hexahydrate as a solution or thin film of Fe deposited on SiO_2 stripes, known to promote suspended growth of long (>100 μm) single-walled carbon nanotubes [25]. After the growth of the CNT above the substrate, it collapses toward the substrate, which initiates a self-coiling due to the tube instability. The final geometry of the CNT is driven by van der Waals interaction between the substrate and preceding loops as described in Refs. [17,23] resulting in a coil with a high-density CNT bundle. The sample grown from ferric chloride hexahydrate (coil 1) was synthesized as detailed in Refs. [23,26] with the following parameters: temperature: 1000 °C, gases: CH_4/H_2 ratio of about 1/5, flow rate: ~54 cm^3/min, and duration: 43 min. The sample grown from evaporated Fe (coil 2) was synthesized as detailed in Ref. [17] with the following parameters: temperature: 900 °C, gases: $Ar:H_2:C_2H_4$ at a ratio of about 60:40:0.02, flow rate: 70–500 cm^3/min, and duration: 45 min.

For the monochiral enriched (6,5) CNT solution, the CoMoCAT SG65i SWCNTs raw powder (SouthWestNanotechnologies, lot no. SG65i-L58) was suspended in water with 1% (m/v) sodium deoxycholate (BioChemica) by tip sonication (WeberUltrasonics, 35 kHz, 16 W in continuous mode) for 1 h. The resulting dispersion was centrifuged at 45 560 g for 1 h and the supernatant collected and used for pH-modulated aqueous two-phase extraction (ATPE) [27] to obtain (6,5) SWCNTs. From this solution, a thin film of highly pure (6,5) carbon nanotubes was prepared using the vacuum filtration method. The homogeneous solution was filtered through a cellulose ester membrane (MCE, 0.025-mm pore size, 25 mm diameter) using a vacuum filtration system at a pressure of 60 kPa. Surfactant removal began during the filtration process using deionized water and isopropyl alcohol. The CNT started to aggregate and were deposited on the filter, dried, cut into 5 × 5 mm pieces, and transferred onto a substrate. The cellulose filter was dissolved by acetone vapor for about 2 h. The filter residuals were removed by placing the sample in liquid acetone, isopropanol, and methanol (each solvent for about 30 min). Samples were dried using a stream of pure nitrogen. Using this method, a film is obtained with high-density packed CNTs.

The structure of our samples was imaged by scanning electron microscopy (SEM), see Supplementary information for details. Coils show a higher SEM contrast than the individual tubes (uncoiled segments connected to the coil), which will be denoted as *tails* or *free ends* in the rest of this paper, see Fig. S1. The coil synthesis method yields coils with dozens of turns in the bundle cross-section. An exhaustive

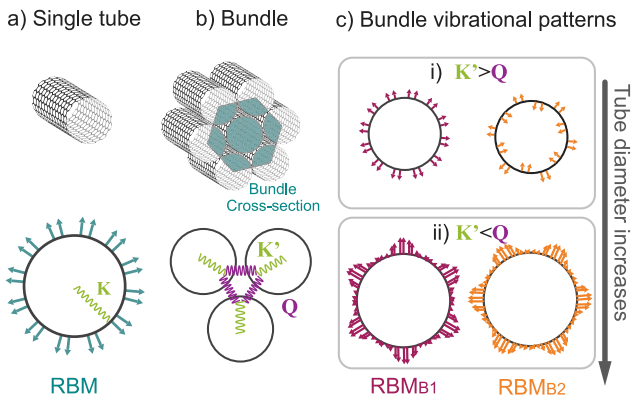

Fig. 1. Representation of the interaction forces and vibrational patterns in single and bundled CNTs. (a) Atomic displacement pattern for RBM in a single isolated tube. (b) Elastic force constants representing the intratube and intertube interactions in a bundle: radial extension (**K′**) and intertube (**Q**). (c) Atomic displacement patterns for infinite bundles. The atomic displacement patterns of the breathing-like modes RBM_{B1} and RBM_{B2} depend on the tube's diameter, according to Popov et al. [22].

description can be found in Ref. [17]. One example is observed in the atomic force microscopy (AFM) image on coil 1, see Fig. S2 A relative comparison of the topographic height of the coil to its free ends provides a rough estimate of the number of turns to be ~80 turns (see Supplementary information for the calculation). The arrangement of the (6,5) CNTs in the film was imaged with SEM. The formation of bundles inside the film is clearly visible in Fig S4. A 2D Fourier transform yields an estimated average bundle thickness of 26 nm. The thickness from both types of bundles corresponds to cross-sections of about 100 nanotubes. This allows us to treat them in the limit of infinite crystals and neglect finite-size effects.

Single excitation wavelength Raman measurements at 638 nm (1.94 eV) were carried out with the Horiba XploRA Raman spectrometer for the coils and film. The characteristic G mode was used to map and locate the coil and the tail. We aligned the polarization of the excitation laser with the main axis of the coils' tail. The bundles in the CNT film did not show a specific orientation, thus no deliberate orientation of the incident light was required.

The resonant Raman spectra of the coil were obtained by a t64000 Horiba spectrometer in a triple-grating configuration equipped with 900 grooves per millimeter grating and a silicon CCD. Fifteen excitation energies between 1.75 to 1.97 eV were used with an intensity ranging from 0.8 to 1.7 mW and with a 2 min integration time. We used an Ar-Kr ion laser (Innova Coherent), a tunable dye laser (Radiant Dyes), and a titanium-Saphire (Ti:Sa) ring laser (Coherent MBR-100) as excitation sources. RBM frequencies were used to estimate the diameter (d) of the CNTs $d = 215\,\mathrm{cm}^{-1}\ \mathrm{nm}/(\omega_{RBM} - 18\,\mathrm{cm}^{-1})$ [28]. All RBMs in the Raman spectra were fitted by a Lorenzian line shape. For the resonance profile, the intensity (defined as the integrated area under the peak) was plotted as a function of the excitation wavelength. The intensity and position of Raman lines were calibrated with respect to the Si peak from the Si/SiO_2 substrate. By fitting the resonance profiles as described in Ref. [28], the transition energy E_{ii} of each RBM mode was calculated.

3. Results and discussion

The radial breathing mode is a unique vibrational feature of CNTs. It describes a breathing-like atomic displacement originating from the symmetric vibration in the radial direction with respect to the tube axis [29]. The phonon eigenvectors of an RBM are shown in Fig. 1a and the mode frequency is inversely proportional to the tube's diameter. When tubes with the same chirality are packed into a two-dimensional hexagonal lattice, they interact via van der Waals forces and generate

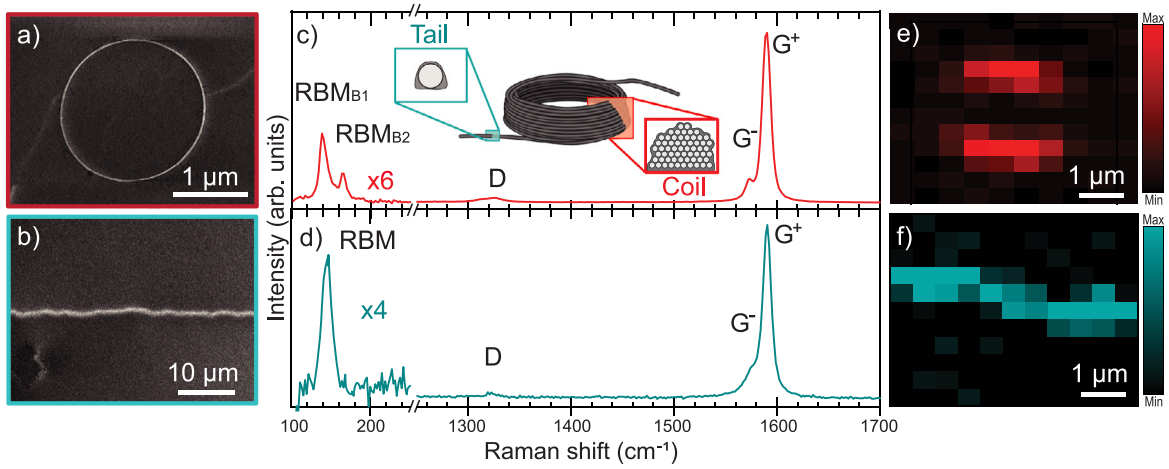

Fig. 2. Structure and Raman spectroscopy of the tail (single tube) and coil (bundle) segments of the defect-free coil 1. (a,b) SEM images of the coil and tail. (c–d) Raman spectra of the coil (red) and the individual-tube tail (blue). Characteristic modes are indicated. (e,f) Raman G mode mapping under 638 nm excitation wavelength. (For interpretation of the references to color in this figure legend, the reader is referred to the web version of this article.)

a coherent and periodic intertube coupling. At the same time, the symmetry is reduced in the crystal compared to a single, isolated tube (Fig. 1b). The lower symmetry of the hexagonal system sustaining the CNT bundle has been predicted to mix the A_{1g} RBM of the isolated tube with a doubly degenerate E normal mode. The mixing results in the generation of two hybrid modes RBM_{B1} and RBM_{B2} in the low-frequency region instead of the single mode characteristic for isolated tubes [22,30]. Popov et al. presented a lattice-dynamical study of infinite cross-sectional bundles of identical tubes using a valence force field (VFF) model with intertube interactions described by the Lennard-Jones potential [22]. The model uses two force constants: the intratube elastic force constant (**K′**) and the intertube interaction force constant (**Q**) (as shown in Fig. 1b). The van der Waals coupling between the nanotubes has the effect of up-shifting the frequency of the intrinsic RBM from the isolated tube. Both modes are fully symmetric within the structure of the CNT crystal and can have mixed vibration patterns, Fig. 1ci. Similarly to the isolated RBM, the collective vibrational modes in CNT bundles were predicted to be diameter-dependent [22]. For small tube radii, **K′** is much larger than **Q**, making the first bundle eigenmode RBM_{B1} practically unchanged compared to the isolated tube's RBM, meanwhile in RBM_{B2} exhibits a stronger shift than RBM_{B1}. As the tube diameter increases, intertube interactions get stronger (**Q**>**K′**) resulting in hexagonal deformations with nearly identical breathing-like shapes for the two bundle modes and correspondingly similar frequencies (see Fig. 1cii) [22]. Similar results were obtained by Dresselhaus et al. [30]. We start our experimental study by measuring a micron-scale carbon nanotube coil with a circular shape and accessible SWCNT ends on both sides. Fig. 2a and b show an SEM image of the coil and one of the free ends, designated as the tail, respectively. By comparing the Raman spectra from the tail and the coil, we identify the effect of bundling on the vibrational properties. Fig. 2c and d show the Raman spectra measured with 1.94 eV excitation energy. Both parts show similar high-frequency D and G modes that we use to further characterize the CNT coil. The G^+ (~1590 cm^{-1}) mode is related to the atomic displacement along the tube axis, the G^- (~1574 cm^{-1}) mode to displacement around the circumference. The Lorentzian line shape with narrow full-width half maximum (FWHM = 5 cm^{-1}) for the G^- peak suggests this to be a semiconducting tube. The disorder-induced D mode (~ 1320 cm^{-1}) was used to examine the density of structural defects before and after coiling. The low D/G integrated intensity ratio of 0.021 indicates the excellent crystallinity of the tube before coiling. The ratio remains constant after the coil is formed (0.023), indicating that coiling does not increase the amount of defects. Fig. 2e and f show Raman maps, where the full Raman spectrum was collected over an area around the coil and tail. The G mode was used to map and locate the coil and the tail. Two maxima lobes are observed for the coil Raman map. They originate from the alignment of coil segments with the horizontal polarization of the exciting laser [14].

The low-energy Raman spectrum (below 500 cm^{-1}) shows significant differences between the coil and the tail. A single RBM peak is observed at 145 cm^{-1} in the tail spectrum, corresponding to an isolated CNT with diameter d = 18 Å. In the coil, the single RBM peak is split into two collective modes, RBM_{B1} = 138 cm^{-1} and RBM_{B2} = 164 cm^{-1}. This change of the low-frequency modes upon packing agrees well with the predictions [22], showing an up-shift of the RBM_{B2} frequency ($_{\Delta}\omega$ = 13 cm^{-1}) and a small shift RBM_{B1} ($_{\Delta}\omega$ = 2 cm^{-1}) with respect to the isolated RBM frequency, see Table 1. However, prior to attributing the effect to bundling we will first confirm that our sample consists of a monochiral CNT to rule out the possibility that these two peaks originate from two different tubes in a single-walled or in a double-walled configuration. The possibility of two RBMs arising from a double-walled CNT can be easily ruled out by comparing the diameter of the "outer" and tentative "inner" tubes. If the two RBMs corresponded to a double-walled CNT, the two constituting tubes would have a diameter difference of 3.2 Å or less. This is smaller than the interlayer distance in graphite (3.5 Å [31]) preventing the CVD growth of such a double-walled tube. Furthermore, according to the Kataura plot, the inner wall would be metallic which is not congruent with the absence of a broad G^- peak characteristic for metallic CNTs [32].

The second possibility is that the two modes arise from the presence of two different SWCNTs coiled together. We can rule this out because different tube chiralities have different transition energies [33] in contrast to the single resonance observed experimentally. We performed multi-wavelength resonant Raman measurements to determine the resonance energies E_{ii} of RBM_{B1} and RBM_{B2} (the RBM signal from the tail was too weak for detection out of resonance) [28,34]. The signal intensity strongly increases when the excitation energy approaches an allowed optical transition reaching its maximum at incoming and outgoing Raman resonances [35], Fig. 3a. We clearly observe how the nanotube gets in and out of resonance, while the line shape and frequency remain constant for both modes. This trend is presented in the two-dimensional plot in Fig. 3b. RBM_{B1} and RBM_{B2} are resonant at the same transition energy, Fig. 3c and thus originate from the same CNT. For RBMs, there is a superposition of the incoming and outgoing resonances due to the small phonon energy (~0.02 eV) [35]. By fitting the resonance profiles of RBM_{B1} and RBM_{B2}, we obtain E_{ii} = 1.84 eV for both modes, confirming the monochiral composition of the coil. Using the Kataura plot and the tube diameter, we assign the resonance

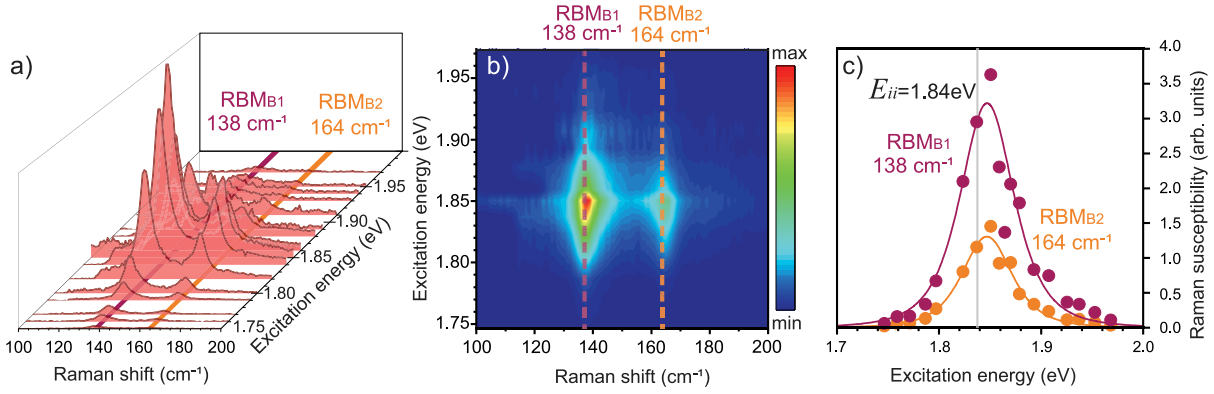

Fig. 3. Low-frequency resonant Raman measurements on coil 1 (a) Raman spectra of the low-frequency region for the nanotube coil from 1.75 to 1.97 eV. Two RBM peaks are observed at 138 and 164 cm^{-1}. The position and line-shape of these peaks remain constant across the entire energy range. (b) 2D Raman excitation map of the two breathing modes from the resonant Raman spectra of coil 1. Both peaks show their maximum intensity at the same energy ~1.84 eV. (c) Resonance excitation profile for the RBM peaks. The dots are the experimental data with solid lines are the best fit to a Raman resonance profile.

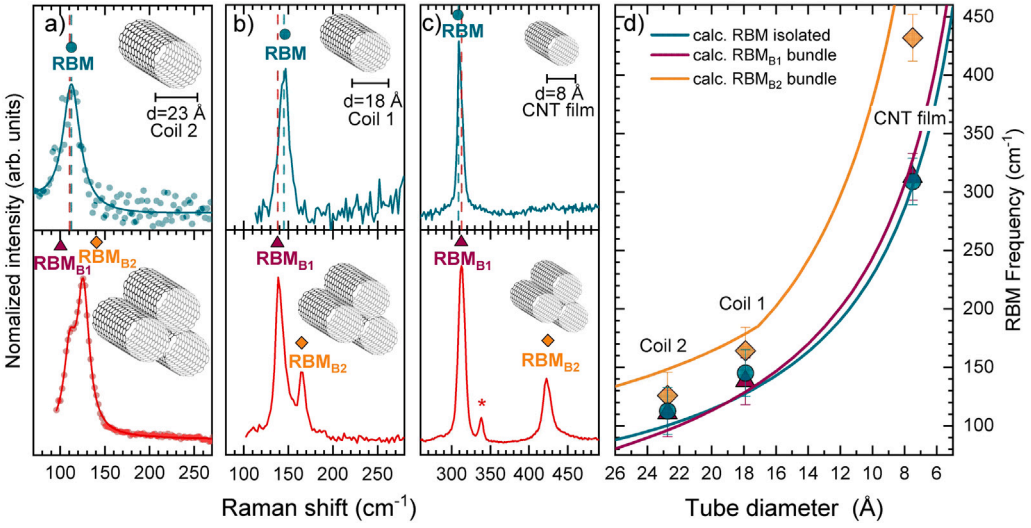

Fig. 4. Diameter dependence of collective vibrational modes. (a–c) Raman spectra of the RBM peaks for single and bundle sections for d = 23, 18, and 7.5 Å samples respectively. ∗ marks an artifact originating from a small number of (6,4) CNTs that have not been removed during the filtration process. (d) Comparison of the observed breathing modes frequency to the theoretical study of infinite bundles of identical nanotubes. Symbols represent the experimental RBM frequencies where circles are RBM frequencies of single tubes, triangles represent RBM_{B1}, and squares RBM_{B2} of bundles [22].

to the E_{33} transition and the chirality to a (14,12) CNT [36]. Compared with the RBM of the tail, RBM_{B2} is shifted to higher frequencies by 19 cm^{-1}, whereas RBM_{B1} is shifted to lower frequencies by 7 cm^{-1}.

To study the diameter dependence of the bundling effect, two additional samples with larger and smaller tube diameters were considered. We first analyzed another coil ("coil 2") made of a tube having a diameter d = 23 Å (calculated from its tail RBM = 112 cm^{-1} peak). An SEM image of this coil is provided in Fig. S3. The low-frequency Raman spectrum of the coil 2 is presented in Fig. 4a. Similarly to the first coil, the second coil shows two RBM peaks, one shifted to higher energies (RBM_{B2}) and one to lower energies (RBM_{B1}) relative to the RBM of the CNT in the tail. The shifts are +13 cm^{-1} and –2 cm^{-1}, respectively. The splitting of the collective RBM decreases in the coil with the large-diameter CNT to Δ_{RBM}(coil 2) = 15 cm^{-1} compared to the Δ_{RBM}(coil 1) = 26 cm^{-1} found in Coil 1, which is made of a smaller-diameter CNT.

A stronger splitting of the bundle's RBM frequencies was predicted for CNT crystals composed of smaller diameter CNTs, but coils with d < 18 Å did not grow in the CVD chamber of our synthesized samples. Instead, we studied a film of racemic (6,5) single-walled carbon nanotubes that are known to result in uniform and densely packed hexagonal crystals of CNT with a tube diameter of 7.5 Å. The top spectrum in Fig. 4c shows the expected (6,5) RBM peak of individual tubes measured in a water-suspended solution at 309 cm^{-1}. Again, two new vibrational modes appear in the bundled section at RBM_{B1} = 313 cm^{-1} and RBM_{B2} = 432 cm^{-1}, with Δ_{RBM} = 119 cm^{-1}, much higher than for coil 1 and 2 with larger diameter tubes. Interestingly, this time RBM_{B1} new vibrational mode in the film is shifted to a higher frequency from the isolated RBM.

The theoretical calculations of Popov et al. characterized the change of the frequencies and spacing between the collective RBM_B modes as a function of tube diameter. They found this trend is the result of a competition between extrinsic and intrinsic interaction forces [22]. Fig. 4d compares our experimental RBM frequencies with the calculations by Popov et al. [22]. The symbols represent the experimental RBM frequencies where circles indicate RBM frequencies of single tubes, triangles mark the RBM_{B1} of bundles, and squares correspond to the RBM_{B2} of bundles. The solid lines represent the theoretical frequencies, with each color denoting a different vibrational mode [37]. Our experimental results align well with theoretical predictions, demonstrating a consistent $1/d$ scaling for all modes, as well as confirming the anticipated up-shift of RBM_{B2} relative to the RBM. We also observe that the peak splitting, Δ_{RBM}, decreases as the tube's diameter increases, confirming a strong agreement between theory and experiment. The simulations predicted a cross-over between RBM and RBM_{B1}, which

Table 1
Summary of all RBM frequencies measured for three CNT diameters on isolated and bundles tubes and comparison to theoretical values for infinite homogeneous bundles [37].

Sample	d	Type	Experiment			Theory	
			RBM	RBM_{B1}	RBM_{B2}	RBM_{B1}	RBM_{B2}
	(Å)	(n,m)	(cm^{-1})	(cm^{-1})	(cm^{-1})	(cm^{-1})	(cm^{-1})
Coil 2	23	–	113	111	126	95	147
Coil 1	18	(14,12)	145	138	164	131	178
CNT film	7.5	(6,5)	309	313	432	319	554

we confirm experimentally. RBM_{B1} shows a nearly pure breathing-like behavior, and the direction of its shift compared to the unbundled RBM is the result of an interplay between the intratube radial-extension force and the intertube interaction force. For small tube diameters (CNT film), we observe an upward shift of the RBM_{B1} ($_{\Delta}\omega = 4$ cm^{-1}). As the diameter increases, the tube elasticity increases and the deformation reduces the radial restoring force $\mathbf{K}'$. The relative intensity of RBM_{B1} decreases and a downshift of 2 cm^{-1} is observed, a trend that is also supported by theoretical predictions [37].

The Raman intensities of the modes, unlike the mode frequencies and frequency differences, are not well reproduced by the single-particle, semi-classical theory [22] in the high and low diameter regions. This can be seen from the relative intensity of RBM_{B2} with respect to RBM_{B1}, see Fig. S5. For the small-diameter CNTs, the calculated intensity of RBM_{B2} almost vanishes for $d < 12$ Å whereas, our measurements show a high-intensity mode with an intensity ratio RBM_{B2}/RBM_{B1} of about 0.4 for $d = 7.5$ Å, Fig. 4c. For the medium-diameter CNTs the ratio of the theoretical RBM_{B2}/RBM_{B1} intensities increases and reaches a maximum of 0.4 at $d = 20$ Å, matching our experimental results, Fig. 4b. For the larger-diameter CNTs the ratio is expected to slightly decrease to 0.3, while in our measurements on the 23 Å diameter coil, the intensity of RBM_{B2} is almost twice the RBM_{B1} intensity (~1.8) Fig. 4a. It is important to note that different calculation models can result in different Raman intensities. For instance, another study based on tight-binding molecular-dynamics calculations also predicted the second breathing-like mode for infinite bundles [30] and showed a different trend for the intensity ratio of the collective modes. The estimated intensity ratio continuously increases with tube diameter, with a value of 0.65 for $d = 18$ Å, and a value of 0.9 for $d = 19$ Å(the largest tube diameter calculated) see Fig. S5, but the simulated diameter range was too small for a comparison with our experimental data. All theoretical studies were performed for infinite CNT crystals. Finite size affects phonon eigenvectors more strongly than the phonon frequency. This may be the reason why the energetic agreement between experiment and theory is much better than for the intensities.

Collective vibrations are a valuable handle for determining the size and quality of CNT bundles in films and other configurations. We have found excellent agreement between theory and experiment in the frequencies of bundled modes. For instance, in the smallest-diameter (6,5) bundles, we observe a substantial contribution from the RBM_{B2} mode, which was not predicted by the initial theory that focused solely on a first-order semi-classical theory [21,22]. This highlights the need for further studies on homogeneous CNT bundles and considering additional interactions such as excitonic effects in collective modes.

In this work, we studied large bundles with $n > 50$ tubes, where finite-size effects are negligible [37]. However, in smaller bundles, finite-size effects are predicted to dominate, leading to changes in the RBM_{B2}/RBM_{B1} ratio and the appearance of more modes in the low-frequency part of the spectrum. Even for two tubes lying side-by-side, moderate effects are expected. Moreover, the theory of collective vibrations can be extended to other types of nanotubes, such as double-walled CNTs [38]. For nanotubes made of materials other than carbon (MoS_2, hBN, etc.), we expect the same effect, but with a different scaling, as elastic constants and atomic masses vary in different materials. Thus various nanotube cylinders can be used to construct and tune phononic crystals of a range of frequencies.

4. Conclusions

We showed that chirally pure nanotubes templated into a phononic crystal display novel vibrational properties manifested in two hybrid breathing-like vibrational modes. This behavior was predicted more than 20 years ago, but has been extremely challenging to observe experimentally due to the difficulties in sorting and synthesis of monochiral and well-packed CNT bundles. We studied two different types of such crystals: coils and films. Two breathing-like modes appeared in the coil, in contrast to the single one found in their unbundled tails. Using resonant Raman spectroscopy we confirmed the two modes arise from a bundling effect of a monochiral CNT bundle by showing the two modes to have the same transition energy. We extended the study to phononic crystals in the limits of large and small tube diameters, revealing that the splitting between the two collective modes decreases with diameter, in agreement with theoretical predictions. In conclusion, chirally pure nanotube bundles represent a novel scheme of THz-range phononic crystals leading to new vibrational modes. Their frequency tunability upon tube diameter offers an excellent tool for the exploration of the collective dynamics of networks of coupled oscillators [39]. This paves the way for the optomechanics field with promising applications in telecommunications and sensors [40].

CRediT authorship contribution statement

Charlotte Berrezueta-Palacios: Investigation, Writing – original draft, Formal analysis, Methodology, Data curation, Visualization. **Dekel Nakar:** Writing – review & editing, Investigation, Resources. **Anna Wroblewska:** Methodology, Writing – review & editing. **Oisín Garrity:** Investigation, Writing – review & editing. **Han Li:** Resources, Writing – review & editing. **Nitzan Shadmi:** Investigation, Writing – review & editing, Resources. **Benjamin S. Flavel:** Writing – review & editing, Supervision, Funding acquisition. **Ernesto Joselevich:** Writing – review & editing, Funding acquisition, Supervision. **Stephanie Reich:** Conceptualization, Funding acquisition, Project administration, Supervision, Writing – review & editing, Formal analysis. **Georgy Gordeev:** Conceptualization, Project administration, Supervision, Writing – review & editing, Formal analysis, Investigation, Writing – original draft.

Declaration of competing interest

The authors declare that they have no known competing financial interests or personal relationships that could have appeared to influence the work reported in this paper.

Acknowledgments

This work was supported by the European Research Council (ERC) under grant DarkSERS-772 108, the German Science Foundation (DFG) under grant 504 656 879 and SupraFAB Research Center at Freie Universität Berlin, Germany. E.J. holds the Drake Family Professorial Chair of Nanotechnology and acknowledges support from the European Research Council (ERC Advanced Grant number 338849), and the Minerva Stiftung, Germany (grant number 713215). This research was also partly supported by the Helen and Martin Kimmel Center for Nanoscale Science, Germany, the Moscowitz Center for Nano and Bio-Nano Imaging, Germany, and the Perlman Family Foundation, Germany. O.G. acknowledges the German Science Foundation (DFG) within the Priority Program SPP 2244 2DMP for funding. H.L. acknowledges support from the Turku Collegium for Science, Medicine and Technology (TCSMT), Germany. B.S.F. gratefully acknowledges support by the DFG, Germany under grant numbers FL 834/5-1, FL 834/7-1, FL 834/9-1 and FL 834/12. G.G. and S.R. acknowledge the Focus Area NanoScale of Freie Universitaet Berlin, Germany.

References

[1] M.S. Kushwaha, P. Halevi, L. Dobrzynski, B. Djafari-Rouhani, Acoustic band structure of periodic elastic composites, Phys. Rev. Lett. 71 (1993) 2022–2025.

[2] V.G. Veselago, The electrodynamics of substances with simultaneously negative values of ϵ and μ, Sov. Phys. Uspekhi 10 (1968) 509–514.

[3] X. Zhang, Z. Liu, Negative refraction of acoustic waves in two-dimensional phononic crystals, Appl. Phys. Lett. 85 (2) (2004) 341–343.

[4] A. Khelif, B. Aoubiza, S. Mohammadi, A. Adibi, V. Laude, Complete band gaps in two-dimensional phononic crystal slabs, Phys. Rev. E 74 (4) (2006) 1–5.

[5] E. Prodan, C. Prodan, Topological phonon modes and their role in dynamic instability of microtubules, Phys. Rev. Lett. 103 (24) (2009) 248101.

[6] S. Mohammadi, A.A. Eftekhar, A. Khelif, W.D. Hunt, A. Adibi, Evidence of large high frequency complete phononic band gaps in silicon phononic crystal plates, Appl. Phys. Lett. 92 (2008) 221905.

[7] J.N. Kirchhof, K. Weinel, S. Heeg, V. Deinhart, S. Kovalchuk, K. Höflich, K.I. Bolotin, Tunable Graphene Phononic Crystal, Nano Lett. 21 (5) (2021) 2174–2182.

[8] J. Paulose, B.G.G. Chen, V. Vitelli, Topological modes bound to dislocations in mechanical metamaterials, Nat. Phys. 11 (2) (2015) 153–156.

[9] B.G. ge Chen, B. Liu, A.A. Evans, J. Paulose, I. Cohen, V. Vitelli, C.D. Santangelo, Topological mechanics of Origami and Kirigami, Phys. Rev. Lett. 116 (2016) 135501.

[10] C.L. Kane, T.C. Lubensky, Topological boundary modes in isostatic lattices, Nat. Phys. 10 (1) (2013) 39–45.

[11] M. Xiao, G. Ma, Z. Yang, P. Sheng, Z.Q. Zhang, C.T. Chan, Geometric phase and band inversion in periodic acoustic systems, Nat. Phys. 11 (3) (2015) 240–244.

[12] Muhammad, C. Lim, Vibration Resonance and Dynamic Characteristics of Pillared Phononic Crystals and Acoustic Metamaterials, in: M.H.F. Aliabadi, W.O. Soboyejo (Eds.), Comprehensive Structural Integrity (Second Edition), second ed., Elsevier, Oxford, 2023, pp. 360–390.

[13] J. Zhu, P. Hu, Y. Chen, S. Chen, C. Zhang, Y. Wang, D. Liu, Waves propagating in nano-layered phononic crystals with flexoelectricity, microstructure, and micro-inertia effects, Nanomaterials 12 (7) (2022) 1080.

[14] C. Thomsen, S. Reich, Raman Scattering in Carbon Nanotubes, in: C. Manuel, R. Merlin (Eds.), Light Scattering in Solids IX, Springer, Berlin Heidelberg, 2007, pp. 164–169, Chapter Raman scat.

[15] Y.H. Yang, W.Z. Li, Radial elasticity of single-walled carbon nanotube measured by atomic force microscopy, Appl. Phys. Lett. 98 (4) (2011) 041901.

[16] S. Reich, C. Thomsen, P. Ordejón, Electronic band structure of isolated and bundled carbon nanotubes, Phys. Rev. B 65 (15) (2002) 155411.

[17] N. Shadmi, A. Kremen, Y. Frenkel, Z.J. Lapin, L.D. Machado, S.B. Legoas, O. Bitton, K. Rechav, R. Popovitz-Biro, D.S. Galvao, et al., Defect-free carbon nanotube coils, Nano Lett. 16 (4) (2016) 2152–2158.

[18] J.J. Crochet, J.D. Sau, J.G. Duque, S.K. Doorn, M.L. Cohen, Electrodynamic and excitonic intertube interactions in semiconducting carbon nanotube aggregates, ACS Nano 5 (4) (2011) 2611–2618.

[19] J.R. Simpson, O. Roslyak, J.G. Duque, E.H. Hároz, J.J. Crochet, H. Telg, A. Piryatinski, A.R.H. Walker, S.K. Doorn, Resonance Raman signature of intertube excitons in compositionally-defined carbon nanotube bundles, Nature Commun. 9 (2018) 637.

[20] A.V. Savin, E.A. Korznikova, S.V. Dmitriev, Plane vibrational modes and localized nonlinear excitations in carbon nanotube bundle, J. Sound Vib. 520 (November 2021) (2022) 116627.

[21] V. Popov, V. Van Doren, M. Balkanski, Elastic properties of crystals of single-walled carbon nanotubes, Solid State Commun. 114 (7) (2000) 395–399.

[22] V.N. Popov, L. Henrard, Evidence for the existence of two breathinglike phonon modes in infinite bundles of single-walled carbon nanotubes, Phys. Rev. B 63 (2001) 233407.

[23] D. Nakar, G. Gordeev, L.D. Machado, R. Popovitz-Biro, K. Rechav, E.F. Oliveira, P. Kusch, A. Jorio, D.S. Galvao, S. Reich, et al., Few-wall carbon nanotube coils, Nano Lett. 20 (2) (2019) 953–962.

[24] A. Wroblewska, G. Gordeev, A. Duzynska, S. Reich, M. Zdrojek, Doping and plasmonic Raman enhancement in hybrid single walled carbon nanotubes films with embedded gold nanoparticles, Carbon 179 (2021) 531–540.

[25] N. Geblinger, A. Ismach, E. Joselevich, Self-organized nanotube serpentines, Nature Nanotechnol. 3 (4) (2008) 195–200.

[26] Q. Wen, W. Qian, J. Nie, A. Cao, G. Ning, Y. Wang, L. Hu, Q. Zhang, J. Huang, F. Wei, Carbon nanotubes: 100 mm long, semiconducting triple-walled carbon nan- otubes (adv. mater. 16/2010), Adv. Mater. 22 (2010).

[27] H. Li, G. Gordeev, O. Garrity, S. Reich, B.S. Flavel, Separation of Small-Diameter Single-Walled Carbon Nanotubes in One to Three Steps with Aqueous Two-Phase Extraction, ACS Nano 13 (2) (2019) 2567–2578.

[28] J. Maultzsch, H. Telg, S. Reich, C. Thomsen, Radial breathing mode of single-walled carbon nanotubes: Optical transition energies and chiral-index assignment, Phys. Rev. B 72 (2005) 205438.

[29] M. Dresselhaus, G. Dresselhaus, R. Saito, A. Jorio, Raman spectroscopy of carbon nanotubes, Phys. Rep. 409 (2) (2005) 47–99.

[30] M.S. Dresselhaus, P.C. Eklund, Phonons in carbon nanotubes, Adv. Phys. 49 (6) (2000) 705–814.

[31] V.N. Popov, L. Henrard, Breathinglike phonon modes of multiwalled carbon nanotubes, Phys. Rev. B 65 (2002) 235415.

[32] A. Jorio, A.G. Souza Filho, G. Dresselhaus, M.S. Dresselhaus, A.K. Swan, M.S. Ünlü, B.B. Goldberg, M.A. Pimenta, J.H. Hafner, C.M. Lieber, R. Saito, *G*-Band resonant Raman study of 62 isolated single-wall carbon nanotubes, Phys. Rev. B 65 (2002) 155412.

[33] C. Fantini, A. Jorio, M. Souza, M.S. Strano, M.S. Dresselhaus, M.A. Pimenta, Optical transition energies for carbon nanotubes from resonant Raman spectroscopy: Environment and temperature effects, Phys. Rev. Lett. 93 (2004) 147406.

[34] G. Gordeev, A. Jorio, P. Kusch, B.G. Vieira, B. Flavel, R. Krupke, E.B. Barros, S. Reich, Resonant anti-Stokes Raman scattering in single-walled carbon nanotubes, Phys. Rev. B 96 (2017) 245415.

[35] Y. Peter, M. Cardona, Fundamentals of Semiconductors: Physics and Materials Properties, Springer Science & Business Media, 2010.

[36] H. Kataura, Y. Kumazawa, Y. Maniwa, I. Umezu, S. Suzuki, Y. Ohtsuka, Y. Achiba, Optical properties of single-wall carbon nanotubes, Synth. Met. 103 (1) (1999) 2555–2558, International Conference on Science and Technology of Synthetic Metals.

[37] L. Henrard, V.N. Popov, A. Rubio, Influence of packing on the vibrational properties of infinite and finite bundles of carbon nanotubes, Phys. Rev. B 64 (20) (2001) 205403.

[38] A. Rahmani, J.-L. Sauvajol, J. Cambedouzou, C. Benoit, Raman-active modes in finite and infinite double-walled carbon nanotubes, Phys. Rev. B 71 (2005) 125402.

[39] G. Heinrich, M. Ludwig, J. Qian, B. Kubala, F. Marquardt, Collective dynamics in optomechanical arrays, Phys. Rev. Lett. 107 (2011) 043603.

[40] T. Vasileiadis, J. Varghese, V. Babacic, J. Gomis-Bresco, D. Navarro Urrios, B. Graczykowski, Progress and perspectives on phononic crystals, J. Appl. Phys. 129 (16) (2021) 160901.